Catalysis Today 164 (2011) 112–118

Contents lists available at ScienceDirect

Catalysis Today

journal homepage: www.elsevier.com/locate/cattod

Core–shell structured nickel and ruthenium nanoparticles: Very active and stable catalysts for the generation of CO_x-free hydrogen via ammonia decomposition

Lianghong Yao [a,b], Tianbao Shi [a], Yanxing Li [a,b], Jin Zhao [a], Weijie Ji [a,*], Chak-Tong Au [b,**]

[a] The Key Laboratory of Mesoscopic Chemistry, Ministry of Education, School of Chemistry and Chemical Engineering, Nanjing University, 22 Hankou Road, Nanjing 210093, China
[b] Department of Chemistry, Center for Surface Analysis and Research, Hong Kong Baptist University, Kowloon Tong, Hong Kong, China

ARTICLE INFO

Article history:
Available online 20 November 2010

Keywords:
Core–shell structure
Nickel
Ruthenium
Nanoparticles
Silica
Ammonia decomposition

ABSTRACT

The present study demonstrates that the silica-encapsulated Ni and Ru nanoparticles (nano-Ni@SiO_2 and nano-Ru@SiO_2) are catalysts more active and stable than the currently known catalysts for the production of CO_x-free hydrogen through ammonia decomposition. The effects of SiO_2 encapsulation are closely related to the nature of the enwrapped core elements. The core size and exposure can be modified upon acid treatment, and the core surface property can also be modified by La or Ce doping. Both approaches result in activity enhancement. The superior performance and stability of the core–shell structures are originated from the unique feature of microcapsular-like reactor.

1. Introduction

For environmental consideration, the on-site generation of hydrogen for proton-exchange membrane fuel cells (PEMFCs) is extremely important [1–6]. The option of hydrogen production directly from carbonaceous substances has its limitations because the CO_x ($x = 1, 2$) side products degrade the cell performance even at extremely low concentrations [7–15]. Alternatively, the direct generation of CO_x-free hydrogen by catalytic ammonia decomposition has been considered [3,5,7–27]. Many metals, alloys, and compounds with noble-metal characters have been studied for such an end [10,17,20–23,27,28–32]. It was found that Ru and Ni are, respectively, the most active among the noble and cheap metals. The carbon nanotubes (CNTs)-supported Ru catalysts are the most outstanding in terms of catalytic activity [23,29–32].

In the last decade, core–shell structured materials have attracted great attentions for their unique structural feature and physicochemical properties [33–35]. Nanoparticles (NPs) coated with silica have been studied in fields such as biology, optics, electronics, magnetism, and sensing [1,11,13–15,36], but hardly in catalysis. With the encapsulation of a nano-material encapsulated in a stable shell, one can have the stability and compatibility of the material enhanced; in the mean time, there could be a change of electron charge, reactivity and functionality of the enwrapped material [37,38].

Ni and Ru NPs are large in specific surface area and hence high in the number of active sites. However, the NPs tend to aggregate into larger particles at elevated temperatures. Our strategy is to have the reactive NPs encapsulated by a porous but stable shell made of inert material such as silica. In the present study, we prepared the core–shell structured nickel and ruthenium NPs, namely, Ni@SiO_2 and Ru@SiO_2 for the production of CO_x-free hydrogen via ammonia decomposition. Investigation of physicochemical properties and catalytic activity of the core–shell catalysts was done by means of N_2 adsorption measurement, XRD, TEM, SEM, H_2-TPR and activity evaluation. It was observed that the catalyst activity and stability of the Ni and Ru NPs can be significantly enhanced by the encapsulation of the NPs with the porous SiO_2 shells.

2. Experimental

2.1. Catalyst preparation

2.1.1. Preparation of NiO and RuO_2 NPs

NiO NPs: Typically, 2.9 g of $Ni(NO_3)_3{\cdot}6H_2O$ (Aldrich, 0.01 mol) was added into 100 ml of distilled water containing 3.0 g of polyethylene glycol (Fluka, PEG-20000). After the solution was stirred for 30 min, 4.5 g of urea was added and the mixture was heated to 85 °C and kept at this temperature for 24 h. The precipitate was collected by centrifugation, washed with ethanol and distilled

* Corresponding author at: Department of Chemistry, Nanjing University, Nanjing 210093, China. Fax: +86 25 83317761.
** Corresponding author. Fax: +852 34117348.
E-mail addresses: jiwj@nju.edu.cn, jiwjnju@yahoo.com (W. Ji), pctau@hkbu.edu.hk (C.-T. Au).

0920-5861/$ – see front matter © 2010 Elsevier B.V. All rights reserved.
doi:10.1016/j.cattod.2010.10.056

water, dried at 100 °C for 10 h, and calcined in air at 400 °C for 4 h. The sample is denoted as nano-NiO hereinafter.

RuO_2 NPs: Typically, 2.1 g of $RuCl_3$ (Aldrich, 0.01 mol) was added to 300 ml of distilled water containing 6.0 g of cyltrimethylammonium bromide (CTAB, ACROS). After 30 min of stirring, the pH of the solution was adjusted to 9 by the slow addition of aqueous ammonia. The mixture was then heated to 60 °C and kept at this temperature for 12 h. The solid product was collected by centrifugation, washed with ethanol and distilled water, dried at 100 °C for 12 h, and calcined in air at 550 °C for 4 h. The sample is denoted as nano-RuO_2 hereinafter.

2.1.2. Preparation of Ni and Ru NPs encapsulated by porous silica shell

0.747 g of NiO or 0.665 g of RuO_2 NPs was added to 50 ml of anhydrous ethanol and subjected to a 30-min supersonic treatment. Then 10 ml of NH_3 H_2O and a designated amount of TEOS (depending on the specific Si/M ratio (M = Ni, Ru)) was added under sonication (1 h) in an ultrasound bath (KQ-100DE, 40 kHz, 100 W). The product was collected by drying at 80–100 °C for 10 h and subjected to *in situ* reduction in a 25% H_2/Ar flow at 550 °C for 2 h. The as-obtained catalysts are denoted as nano-Ni@SiO_2 or nano-Ru@SiO_2 hereinafter.

We did not measure the loading of Ni and Ru in nano-M@SiO_2 using elemental analysis such as ICP-OES with the consideration that the use of HF acid to dissolve sample may cause Si loss. Instead, we adopt a specific preparation procedure to achieve SiO_2 coating. Based on this preparation approach (see above), there is no filtration but only gentle evaporation applied; therefore, the components of Ni, Ru, and Si are essentially preserved in the final catalyst, and their contents should be equivalent or very close to the nominal values used in preparation.

2.1.3. Preparation of the doped nano-Ni@SiO_2

The NiO NPs were first impregnated with the solution of a specific dopant followed by silica encapsulation. As an example, the nano-Ni + 0.1Ce@SiO_2 (Si/Ni = 0.2) was prepared as follows: 0.434 g of $Ce(NO_3)_3{\cdot}6H_2O$ was dissolved in 30 ml of anhydrous ethanol under stirring. After 30 min, 0.747 g of NiO NPs was added into the solution. The suspension was stirred for 2 h, and then dried at 100 °C for 10 h and calcined in air at 300 °C for 3 h. The obtained material was then added to 50 ml of anhydrous ethanol and subjected to 30-min supersonic treatment. Subsequently, 10 ml of NH_3 H_2O and 0.45 ml of TEOS was added under sonication (1 h), and the mixture was brought to dryness in an oven at 80 °C for 10 h. The as-obtained product was subjected to *in situ* reduction in a 25% H_2/Ar flow at 550 °C for 2 h. The catalyst obtained in such a way is denoted as nano-Ni + *x*M@SiO_2 (M = doped element, *x* = M/Ni ratio) hereinafter.

2.2. Characterization

The specific surface area of the samples was measured on a NOVA1200 apparatus. Prior to N_2 adsorption, the samples were degassed at 300 °C for 3 h. XRD analysis was performed on a Philips X'Pert MPD Pro X-ray diffractometer, with graphite monochromatized Cu Kα radiation (λ = 0.1541 nm). TEM images were taken on a JEM-1010 TEM microscope operated at 200 kV. High resolution TEM (HRTEM) images were recorded on a FEI Tecnai G2 20S-twin transmission electron microscope. SEM images were taken on a LEO 1450VP scanning microscope. H_2-TPR was carried out in the range of room temperature (RT) to 1000 °C. 50 mg of sample was reduced in a flow of 5% H_2/N_2 (40 ml/min) at a heating rate of 10 °C/min. H_2-TPD was carried out to estimate the surface exposure of metallic cores.

2.3. Catalytic activity

Catalytic testing was carried out in a continuous-flow quartz reactor (catalyst: 100 mg, 60–80 mesh) under pure NH_3 (flow rate = 50 ml/min). Before the reaction, the catalyst was reduced *in situ* in a 25% H_2/Ar flow at 550 °C for 2 h, then purged with a flow of pure Ar. The reaction temperature was in the range of 400–700 °C. The acquisition of activity data at a particular temperature was conducted after the establishment of steady state. Product analysis was performed on an on-line gas chromatograph (Shimadzu or GC122) equipped with thermo-conductive detector and Poropak Q column, using He as a carrier gas. NH_3 conversion in a blank reactor was <1.0% at 550 °C.

3. Results and discussion

3.1. BET measurement

Shown in Table 1 are the BET surface areas of the nano-NiO@SiO_2, nano-Ru_2O_3@SiO_2 and doped catalysts with different Si/Ni and Si/Ru ratios. It seems that the type of core element determines the dispersion as well as encapsulation state of core particles, which in turn affects on the surface area of nano-M@SiO_2. The adhesion of RuO_2 particles is more significant than NiO counterparts (see Section 3.2). Compared with the naked Ni and Ru NPs, the nano-M@SiO_2 (M = Ni, Ru) samples have higher specific surface areas (Table 1), this is due to the presence of SiO_2 shell and its porosity. At the same Si/M ratio, the contribution of SiO_2 shell to total surface area in nano-NiO@SiO_2 is a bit higher than that in nano-RuO_2@SiO_2. With increasing Si/M ratio, the surface area of sample is not increased accordingly, suggesting that the texture and core–shell contact could change at higher Si/M ratio. In addition, the surface area of acid treated nano-RuO_2@SiO_2 is slightly decreased. The mild acid treatment has little effect on the porosity of SiO_2 shell, but can diminish the RuO_2 size due to the acid dissolution, and the resulting salt species can be redistributed in the micropores of SiO_2 shell. The overall consequence is a slight decrease in the surface area of acid treated nano-RuO_2@SiO_2.

3.2. TEM

Fig. 1 shows the TEM images of the core–shell structured samples. The diameters of NiO and RuO_2 cores are in the range of 20–50 nm. At Si/M ratio = 0.2–0.4, the SiO_2 shell is approximately 5–10 nm in thickness. It is thought that there is little diffusion limitation in such a thin and porous SiO_2 layer. Note that there is structure complexity for different core–shell structured catalysts. For instance, although RuO_2 seems smaller than NiO in the primary particle size, the aggregation of RuO_2 particles is more significant than NiO counterparts, and there is obvious trend in forming the "multi-core" encapsulation for nano-RuO_2@SiO_2. After *in situ* reduction, the Ni and Ru cores seem comparable in particle size (Fig. 2e vs. f). On the other hand, the thickness and coverage

Table 1
Surface areas of samples before reaction.

Catalyst	Surface area (m^2/g)
Nano-NiO	85
Nano-NiO@SiO_2 (Si/Ni = 0.2)	112
Nano-NiO@SiO_2 (Si/Ni = 0.4)	101
Nano-RuO_2	24
Nano-RuO_2@SiO_2 (Si/Ru = 0.2)	42
Nano-RuO_2@SiO_2-citric acid (Si/Ru = 0.2)	30
Nano-RuO_2@SiO_2 (Si/Ru = 0.4)	44
Nano-RuO_2@SiO_2 (Si/Ru = 0.6)	38

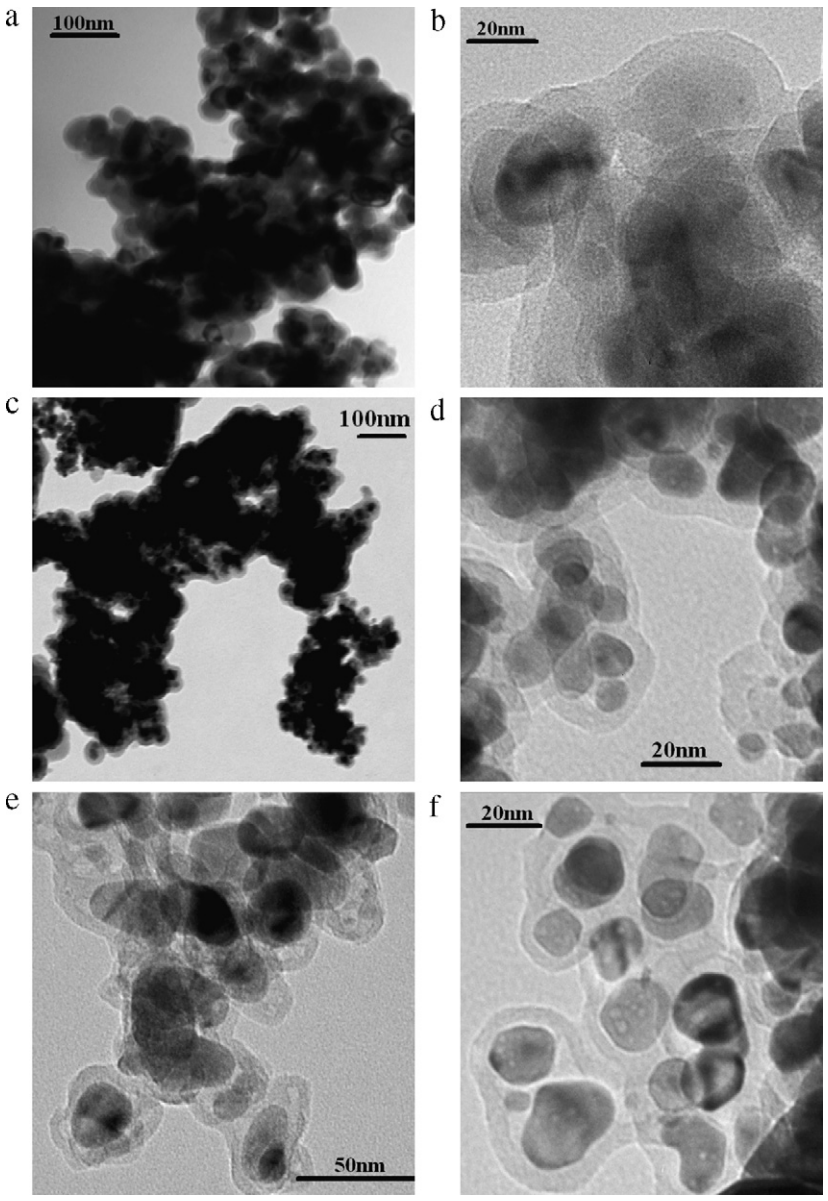

Fig. 1. TEM and HRTEM images of the core–shell structured samples. (a) TEM, nano-NiO@SiO_2, Si/Ni = 0.4; (b) HRTEM, nano-NiO@SiO_2, Si/Ni = 0.2; (c) TEM, nano-RuO_2@SiO_2, Si/Ru = 0.4; (d) HRTEM, nano-RuO_2@SiO_2, Si/Ru = 0.2; (e) HRTEM, nano-Ni@SiO_2 (Si/Ni = 0.2); (f) HRTEM, nano-Ru@SiO_2 (Si/Ru = 0.2).

of SiO_2 shell could be different for nano-RuO_2@SiO_2 and nano-NiO@SiO_2. The SiO_2 shell in nano-NiO@SiO_2 is apparently thicker than that in nano-RuO_2@SiO_2 (Fig. 2b vs. d), which may partly account for the higher surface area of nano-NiO@SiO_2 compared to nano-RuO_2@SiO_2 (due to larger contribution of thicker SiO_2 shell to overall surface area of sample).

3.3. XRD

Figs. 2 and 3 show the XRD results of the core–shell structured catalysts before and after H_2 treatment (550 °C for 2 h in 25% H_2/Ar). In the cases of NiO@SiO_2 (0, 0.1, 0.2, 0.4), the XRD patterns show the NiO phase only (Fig. 2a). After H_2-treatment, the XRD patterns indicate the existence of the metallic Ni phase (Fig. 2b). It is observed that the intensity and width of reflections of NiO as well as Ni in the composites with SiO_2 layers change with Si/Ni content. We deduced that there is variation in NiO dispersion during SiO_2 encapsulation with different Si/Ni ratios. In the present study, SiO_2 encapsulation of NiO NPs is achieved in a NiO suspension of anhydrous ethanol which contains NH_3 H_2O and different amount of TEOS under sonication. Supersonic treatment can likely increase NiO dispersion while higher content of TEOS in suspension (increasing Si/Ni ratio) may reduce such an effect. The overall consequence turns out a variation in NiO dispersion at different Si/Ni ratios and shows an impact on the intensity and width of reflections of NiO. The metallic Ni cores are obtained upon NiO reduction in the core–shell structure; therefore, the dispersion of NiO also determines the dispersion of Ni. As for the serial RuO_2@SiO_2 (0.1, 0.2, 0.4, 0.6) samples, only the signals of the RuO_2 phase are observed (Fig. 3a). After H_2-reduction, only metallic Ru phase exists (Fig. 3b).

It is noted that because of the core–shell structure, the cores are encapsulated by SiO_2 layers, it is difficult to measure the core property by surface science technique such as XPS.

3.4. H_2-TPR

Fig. 4 shows the H_2-TPR profiles of the nano-NiO@SiO_2 (Si/Ni = 0.2) and nano-RuO_2@ SiO_2 (Si/Ni = 0.2) samples. It is appar-

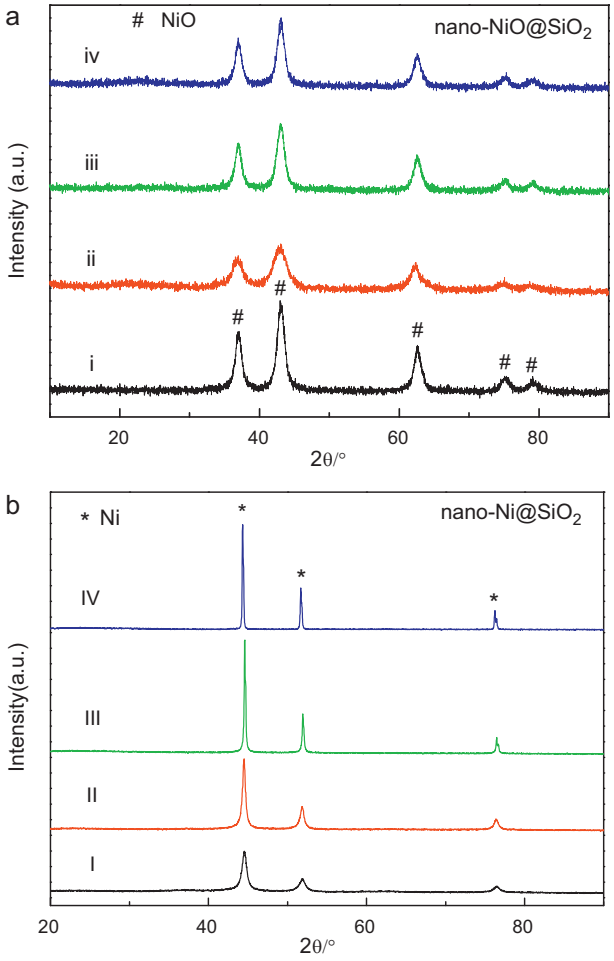

Fig. 2. XRD patterns of (a) nano-NiO@SiO_2 and (b) nano-Ni@SiO_2 at different Si/Ni ratios. (i) Si/Ni = 0; (ii) Si/Ni = 0.1; (iii) Si/Ni = 0.2; (iv) Si/Ni = 0.4; (I) Si/Ni = 0; (II) Si/Ni = 0.1; (III) Si/Ni = 0.2; (IV) Si/Ni = 0.4.

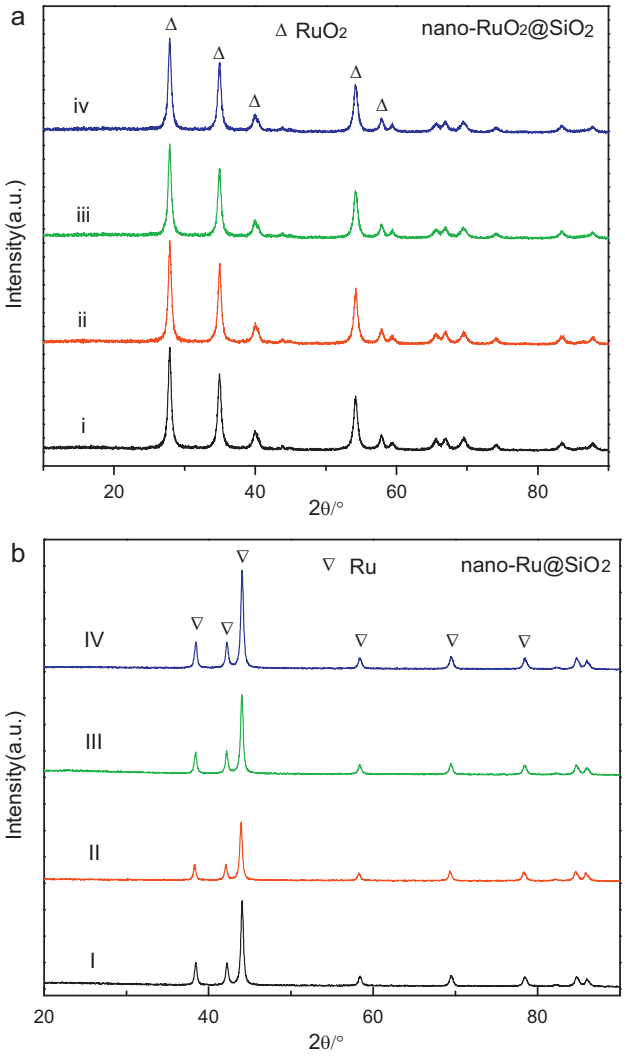

Fig. 3. XRD patterns of (a) nano-RuO_2@SiO_2 and (b) nano-Ru@SiO_2 NPs at different Si/Ru ratios. (i) Si/Ru = 0.1; (ii) Si/Ru = 0.2; (iii) Si/Ru = 0.4; (iv) Si/Ru = 0.6; (I) Si/Ru = 0.1; (II) Si/Ru = 0.2; (III) Si/Ru = 0.4; (IV) Si/Ru = 0.6.

ent that the RuO_2 cores are more easily reduced than the NiO cores, in agreement with our previous observation made on NiO/MCM-41 (IMP) and RuO_2/MCM-41 (IMP) samples [24]. In the cases of the core–shell catalysts, there is the detection of only one symmetric reduction peak, for the MCM-41 supported NiO and RuO_2 NPs, there are several reduction peaks [24]. The TPR results imply that (i) the core–shell interaction is dependent upon core constitution; and (ii) the particle size distribution of NiO and RuO_2 in the core–shell structures differs from that in the supported systems.

Note that the reduction peaks of the La- and Ce-doped NiO@SiO_2 (Si/Ni = 0.2) samples increase in intensity and the peak temperatures notably shifted toward the lower end (Fig. 4b). The behaviors suggest that the doped components can significantly modify the reduction property of the core oxide NPs.

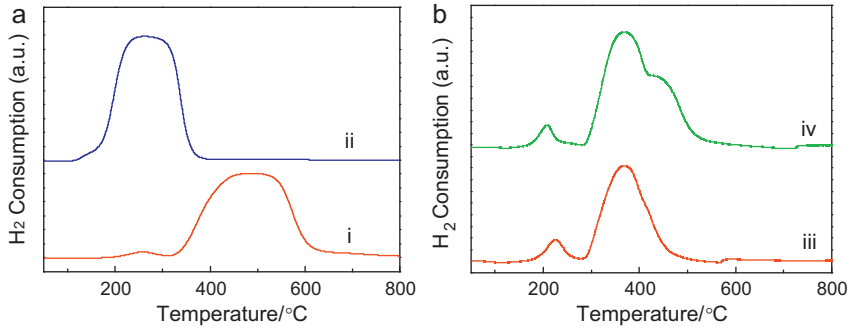

Fig. 4. TPR profiles of (a) nano-NiO@SiO_2 (Si/Ni = 0.2) and nano-RuO_2@SiO_2 (Si/Ru = 0.2) (i and ii, respectively), and (b) nano-NiO + 0.1La@SiO_2 and (b) nano-NiO + 0.1Ce@SiO_2 (Si/Ni = 0.2) (iii and iv, respectively).

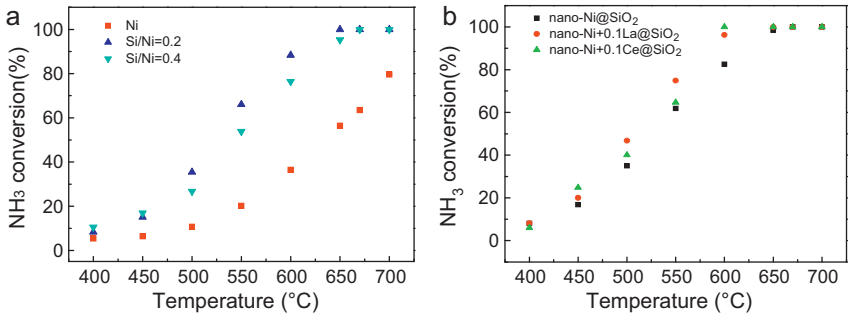

Fig. 5. Temperature dependence of ammonia conversion over (a) Ni NPs and nano-Ni@SiO_2 of different Si/Ni ratios, (b) nano-Ni@SiO_2 and La- and Ce-modified nano-Ni@SiO_2.

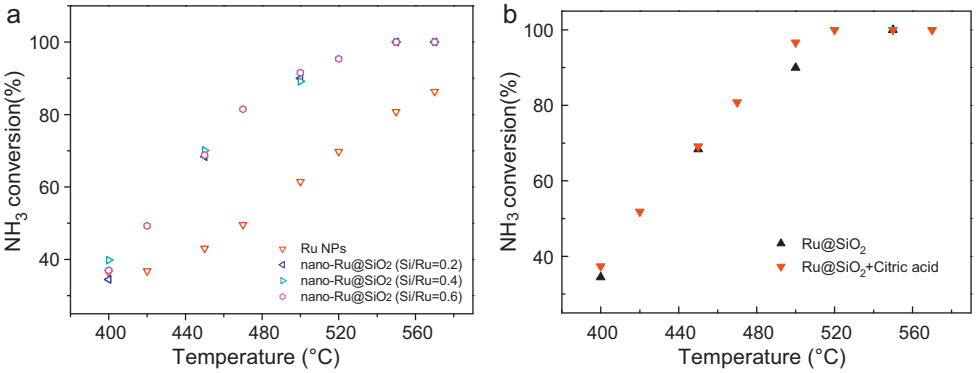

Fig. 6. Temperature dependence of ammonia conversion over (a) Ru NPs and nano-Ru@SiO_2 of different Si/Ru ratios, (b) nano-Ru@SiO_2 (Si/Ru = 0.2) and citric acid treated nano-Ru@SiO_2 (Si/Ru = 0.2).

3.5. Catalytic performance

3.5.1. Ni@SiO_2 and doped Ni@SiO_2

We correlated the catalytic activity with catalyst characteristics on different bases. The catalytic activities are compared based on the NH_3 conversions (Figs. 5 and 6), the H_2 formation rates (Table 2, normalized to per gram of catalyst as well as to per gram of metal), and the TOF values of H_2 production (Table 3, the intrinsic activities normalized to per surface metal atom determined by H_2-TPD investigation). In other words, the catalytic behaviors of nano-M@SiO_2 catalysts have been interpreted in terms of different catalyst characters.

Fig. 5a shows the ammonia conversions over Ni@SiO_2 (0, 0.2, 0.4) at elevated reaction temperatures. Compared with the naked Ni NPs, the core–shell catalysts show significantly higher NH_3 conversions in the 500–700 °C range. Among the Ni@SiO_2 (0.2, 0.4) catalysts, the Ni@SiO_2 (0.2) shows the best performance for ammonia decomposition. The results suggest that the core–shell structures are superior to the naked Ni NPs, and the Si/Ni ratio adopted in catalyst preparation has an effect on catalyst performance. It is possible that the Si/Ni ratio may have an impact on the porosity of the shells, and consequently affecting the core exposure as well as the diffusion efficiency of the reactant and products. The present study included the preliminary activity data of La-, Ce-doped catalysts for comparison. The effect of La and Ce doping on the physicochemical property of core–shell catalyst is systematically studied and the results are to be published separately. Nevertheless, it is observed that introduction of La and Ce dopants

Table 2
H_2 formation rates on the basis of per unit mass of catalyst (mmol/(min g_{cat})) and per unit mass of metal (mmol/(min g_{metal}), in parentheses) over various catalysts.

Catalyst	Temp. (°C)					
	400	450	500	550	600	650
Nano-Ni	1.8 (2.3)	2.2 (2.8)	3.6 (4.6)	6.8 (8.7)	12.2 (15.5)	18.9 (24.1)
Nano-Ni@SiO_2 (Si/Ni = 0.2)[a]	2.7 (4.0)	5.6 (8.3)	11.7 (17.3)	20.7 (30.6)	27.6 (40.8)	33.0 (48.7)
Nano-Ni@SiO_2 (Si/Ni = 0.4)	3.5 (5.9)	5.7 (9.6)	8.9 (15.0)	18.0 (30.3)	25.6 (43.0)	31.9 (53.6)
Nano-Ni + 0.1La@SiO_2	2.7 (4.7)	6.7 (11.8)	15.7 (27.5)	25.1 (44.0)	32.2 (56.5)	33.5 (58.8)
10% Ni/SiO_2 [16]	0.4 (4.0)	1.3 (13.0)	3.3 (33.0)	6.8 (68.0)	11.4 (114)	21.1 (211)
65% Ni/SiO_2-Al_2O_3 [16]	1.1 (1.7)	2.9 (4.5)	6.8 (10.5)	15.2 (23.4)	24.9 (38.3)	30.3 (46.6)
Ni/MCM-41(TIE) [24]	2.1 (29.2)	4.0 (55.6)	8.9 (124)	15.9 (221)	24.0 (333)	30.6 (425)
Nano-Ru	12.2 (16.1)	14.4 (19.0)	20.6 (27.1)	27.1 (35.7)	28.9 (38.1)	30.5 (40.2)
Nano-Ru@SiO_2 (Si/Ru = 0.2)	11.5 (16.5)	22.9 (32.9)	30.1 (43.2)	33.5 (48.1)	33.5 (48.1)	33.5 (48.1)
Nano-Ru@SiO_2 (Si/Ru = 0.4)	13.3 (20.7)	23.5 (36.5)	29.9 (46.5)	33.5 (52.1)	33.5 (52.1)	33.5 (52.1)
Ru/Al_2O_3-w [31]	0.6 (12.5)	1.9 (39.6)	5.6 (117)	11.5 (240)	–	–
Ru/MCM-41(IMP) [24]	6.9 (138)	14.2 (284)	23.9 (478)	31.7 (634)	–	–

[a] Si/Ni (Ru) molar ratio.

Table 3
TOF_{H_2} (s^{-1}) over the nano-Ni@SiO_2, nano-Ru@SiO_2, and reference catalysts.

Catalyst	Temp. (°C)					
	400	450	500	550	600	650
Nano-Ni@SiO_2 (Si/Ni = 0.2)[a]	1.5	3.1	6.5	11.5	15.3	18.3
10% Ni/SiO_2 [16]	0.5	1.4	3.5	7.1	11.9	22.1
65% Ni/SiO_2–Al_2O_3 [16]	<0.1	<0.1	0.1	0.2	0.4	0.5
K-Ni/MCM-41 (IMP) [24]	0.6	1.0	1.7	2.9	4.3	5.5
K-Ni/MCM-41 (TIE) [24]	0.3	0.5	1.0	1.6	2.3	2.9
Nano-Ru@SiO_2 (Si/Ru = 0.2)	6.9	13.8	18.1	20.2	–	–
Ru/Al_2O_3-w [31]	0.4	1.1	3.3	6.9	–	–
K-Ru/MCM-41 (IMP) [24]	2.8	5.0	7.2	8.2	–	–

[a] Si/Ni (Ru) molar ratio.

to nano-M@SiO_2 enhanced the dispersion of core NPs in the SiO_2 shells and also promoted the reduction of encapsulated metal oxide particles to metallic entities. It is also observed that the dopants are presented on the cores as well as in the pores of SiO_2 shells upon *in situ* H_2 reduction. With dopants introduction, there is little change in the lattice parameters of NiO and no new phase detected, also suggesting that the dopants are presented on the core surface rather than in bulk. Fig. 5b demonstrates that the La and Ce doping of nano-Ni@SiO_2 (0.2) can notably promote the reaction. The nano-Ni + 0.1Ce@SiO_2 catalyst gives 100% NH_3 conversion at 600 °C, much more active than the Ni catalyst supported on MCM-41 at the same reaction temperature (71.6% NH_3 conversion) [24]. To the best of our knowledge, this is the best performance known for NH_3 decomposition over Ni-based catalysts. The results also suggest that the doping effect is determined by the nature of dopants.

3.5.2. *Ru@SiO_2 and acid treated Ru@SiO_2*

Fig. 6a shows the temperature dependence of NH_3 conversion over the naked Ru NPs and the core–shell structured Ru@SiO_2 (0.2, 0.4, 0.6). It is clear that the core–shell structured catalysts are much more active than the naked Ru NPs. Note that the naked Ru NPs and the encapsulated Ru NPs are significantly more active than the Ni counterparts, respectively. Over nano-Ru@SiO_2, 100% NH_3 conversion can be achieved at 550 °C with GHSV = 30,000 ml/g h. The Si/Ru ratio adopted in catalyst preparation has little influence on the performance, and it is understandable because there is the formation of hierarchical SiO_2 shells as revealed in TEM observations (Fig. 1). Fig. 6b demonstrates the effect of citric acid treatment on nano-Ru@SiO_2 (Si/Ru = 0.2). There is a positive effect on catalytic performance as a result of the acid treatment, and this can be interpreted as the consequence of increase in spacing of the hierarchical SiO_2 shells as well as enhancement in exposure of the Ru cores.

3.5.3. *H_2 formation rates and TOFs*

Depicted in Table 2 are the H_2 formation rates over the naked Ni and Ru NPs, the core–shell structured nano-Ni@SiO_2 and nano-Ru@SiO_2, as well as that over the La-doped nano-Ni@SiO_2 catalysts. For the purpose of comparison, the data derived over the silica-supported 10% Ni/SiO_2 [16], 65% Ni/SiO_2-Al_2O_3 [16], Ni/MCM-41(TIE) [24], Ru/Al_2O_3-w [31], Ru/MCM-41(IMP) catalysts [24] at 600 °C are also included in the table. The H_2 formation rates are calculated on the basis of both per unit mass of catalyst and per unit mass of metal (using nominal metal contents, see in parentheses of Table 2). One can see that on the basis of per unit mass of catalyst, the core–shell structured catalysts are significantly more active than the naked counterparts. The H_2 formation rates at 600 °C observed over the nano-Ni@SiO_2 (Si/Ni = 0.2) and nano-Ni + 0.1La@SiO_2 catalysts are 27.6 and 32.2 mmol/(min g_{cat}), respectively, while that reported over Ni/MCM-41(TIE) is 24.0 mmol/(min g_{cat}) [24]. The nano-Ru@SiO_2 is also superior to the Ru/MCM-41 (IMP) catalyst. One should make the comparison with caution among these catalysts because the metal loadings as well as dispersions are different across the catalysts. Due to the unique structure and higher metal content of the core–shell catalysts, the H_2 formation rates of nano-M@SiO_2 are lower than that of supported catalysts on the basis of per unit mass of metal (Table 2, the values in parentheses).

Based on the peak area of the H_2-TPD profiles and assuming an adsorption of one H atom per metal atom [16], the H_2 chemisorption uptakes can be estimated by referring to the result acquired in a standard procedure of CuO reduction. In terms of the amount of exposed atoms, the activities are also compared on the basis of TOF values obtained over the representative catalysts reported in the present study and literature. The TOF value of nano-Ru@SiO_2 (Si/Ni = 0.2) is much higher than that of nano-Ni@SiO_2 (Si/Ni = 0.2), which is attributable to the intrinsic chemical nature of Ru. Over the Ru catalysts, the B5 sites (with five nearest neighbors) were proposed for the reaction [39]. The density of such kind of sites may vary with factors such as the dispersion of core particles and the core–shell interaction. On the other hand, the TOF values of nano-M@SiO_2 are essentially higher than that of a few examples of supported catalysts in the 400–600 °C range (Table 3), suggesting that core–shell structured catalyst is intrinsically more active than supported catalyst.

Based on the Arrhenius plots (not shown), one can obtain the apparent activation energies (E_a) for ammonia decomposition over the core–shell structured nano-Ni@SiO_2 and nano-Ru@SiO_2 catalysts. Compared the E_a values of nano-Ni@SiO_2 (63.4 kJ/mol) and nano-Ru@SiO_2 (41.2 kJ/mol) with that of Ni/CNTs (90.3 kJ/mol) [24], K-Ni/MCM-41(IMP) (53.5 kJ/mol) [24], as well as with that (varied from 83.6 to 92.0 kJ/mol) of 10% Ni loading on SiO_2, HY and HZSM-5, and 65% Ni loading on SiO_2–Al_2O_3 [16], one can see that the E_a values derived in the present study are reasonable in reflecting the intrinsic catalytic behavior of the catalysts.

The stability of nano-Ni@SiO_2 and nano-Ru@SiO_2 catalysts was tested under certain reaction conditions. Both show excellent sta-

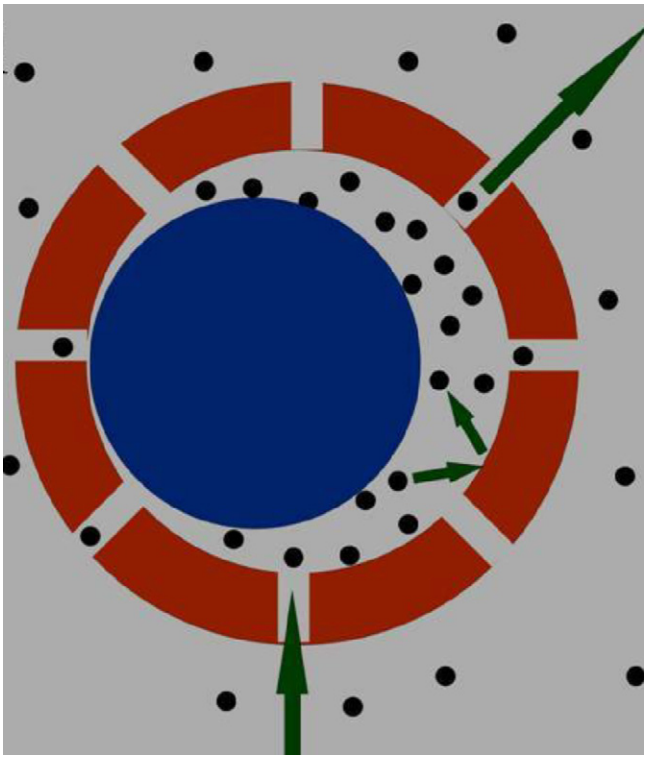

Fig. 7. Illustration of enhanced adsorption and reaction in a core–shell structured microcapsular-like reactor.

bility even subject to a running at 650 °C for 45 h. On the other hand, the naked NPs shows obvious deactivation (>15% reduction in NH_3 conversion) within a period of 65 h due to the lack of the stable shell that prevents the nano-cores from aggregation during reaction.

The space between SiO_2 shell and metal core is created due to the reduction of metal oxide cores to metallic ones. Such spacing is experimentally evidenced in Fig. 2e and f. Note that there are multi-core encapsulations (a few cores encapsulated in one shell) for nano-NiO@SiO_2 and nano-RuO_2@SiO_2 (especially the latter), therefore, re-dispersion of Ni and Ru NPs in the hierarchical SiO_2 shells could occur during *in situ* reduction of the catalyst precursors, which in turn can modify the space between SiO_2 shell and metal core. Nevertheless, the HRTEM images of nano-M@SiO_2 (M = Ni, Ru) (Fig. 2e and f) clearly indicated the spacing which is also schematically illustrated in Fig. 7. Our recent study revealed that the presence of such spacing is curial for superior performance of core–shell catalyst [40]. Therefore, the core–shell nanostructures provide unique environment around the cores which can function as microcapsular-like reactor [40,41] in which the reactant molecules are enriched (confinement effect). Similar phenomenon has been reported recently over the carbon nanotubes encapsulated Fe nanoparticles [42]. As a result, adsorption and catalytic reaction are enhanced on the core surfaces (Fig. 7). In other words, despite there is a decline in exposure of surface metal atoms on the basis of per unit mass of metal, the core–shell catalysts seem intrinsically more active than the naked metal NPs or conventional supported ones.

4. Conclusions

The present study demonstrates that the Ni and Ru NPs encapsulated in silica shells are the most active catalysts known to date for CO_x-free hydrogen production through ammonia decomposition. It is observed that the encapsulation state of SiO_2 shell is closely related to the nature of cores. There is an obvious trend to form "multi-core" encapsulation in the cases of RuO_2@SiO_2 and Ru@SiO_2 nanostructures. Acid treatment and doping of rare earth element La or Ce are the means to modify the property of the core–shell catalysts, and the approaches showed positive consequence. The superior performance and stability of the core–shell structures is originated from the unique character of microcapsular-like reactor.

Acknowledgement

We acknowledge the financial support of the RGC, HKSAR (RGC 200107).

References

[1] M. Danek, K.F. Jensen, C.B. Murray, M.G. Bawendi, Chem. Mater. 8 (1996) 173–180.
[2] R.Z. Sorensen, L.J.E. Nielsen, S. Jensen, O. Hansen, T. Johannessen, U. Quaade, C.H. Christensen, Catal. Commun. 6 (2005) 229–232.
[3] S.F. Yin, B.Q. Xu, X.P. Zhou, C.T. Au, Appl. Catal. A 277 (2004) 1–9.
[4] R. Metkemeijer, P. Achard, Int. J. Hydrogen Energy 19 (1994) 535–542.
[5] R. Metkemeijer, P. Achard, J. Power Sources 49 (1994) 271–282.
[6] W. Arabczyk, J. Zamlynny, Catal. Lett. 60 (1999) 167–171.
[7] W. Arabczyk, U. Narkiewicz, Appl. Surf. Sci. 196 (2002) 423–428.
[8] J. Hepola, P. Simell, Appl. Catal. B 14 (1997) 287–303.
[9] P.A. Simell, J.O. Hepola, A.O. Krause, Fuel 76 (1997) 1117–1127.
[10] G. Papapolymerou, V. Bontozoglou, J. Mol. Catal. A: Chem. 120 (1997) 165–171.
[11] X. Peng, M.C. Schlamp, A.V. Kadavanich, A.P. Alivisatos, J. Am. Chem. Soc. 119 (1997) 7019–7029.
[12] M.L. Breen, A.D. Dinsmore, R.H. Pink, S.B.B.R. Qadri, Ratna, Langmuir 17 (2001) 903–907.
[13] P. Reiss, J. Bleuse, A. Pron, Nano Letters 2 (2002) 781–784.
[14] V. Skumryev, S. Stoyanov, Y. Zhang, G. Hadjipanayis, D. Givord, J. Nogues, Nature 423 (2003) 850–853.
[15] H. Zeng, J. Li, Z.L. Wang, J.P. Liu, S.H. Sun, Nano Letters 4 (2004) 187–190.
[16] T.V. Choudhary, C. Svadinaragana, D.W. Goodman, Catal. Lett. 72 (2001) 197–201.
[17] W. Rarog, Z. Kowalczyk, J. Sentek, D. Skladanowski, D. Szmigiel, J. Zielinski, Appl. Catal. A 208 (2001) 213–216.
[18] W. Raróg, D. Szmigiel, Z. Kowalczyk, S. Jodzis, J. Zielinski, J. Catal. 218 (2003) 465–469.
[19] A. Jedynak, Z. Kowalczyk, D. Szmigiel, W. Raróg, J. Zielinski, Appl. Catal. A 237 (2002) 223–226.
[20] D.A. Goetsch, S.J. Schmit, WO Patent 0,187,770 (2001).
[21] K. Kordesch, V. Hacker, R. Fankhauset, G. Faleschini, WO Patent 0,208,117 (2002).
[22] M.E.E. Abashar, Y.S. Al-Sughair, I.S. Al-Mutaz, Appl. Catal. A 236 (2002) 35–53.
[23] S.F. Yin, Q.H. Zhang, B.Q. Xu, W.X. Zhu, C.F. Ng, C.T. Au, J. Catal. 224 (2004) 384–396.
[24] X.K. Li, W.J. Ji, J. Zhao, S.J. Wang, C.T. Au, J. Catal. 236 (2005) 181–189.
[25] K. Hashimoto, N. Toukai, J. Mol. Catal. A: Chem. 161 (2000) 171–178.
[26] M.C.J. Bradford, P.E. Fanning, M.A. Vannice, J. Catal. 172 (1997) 479–484.
[27] H. Dietrich, K. Jacobi, G. Ert, Surf. Sci. 352 (1996) 138–141.
[28] C. Boffito, J.D. Baker, WO Patent 9,840,311 (2002).
[29] S.F. Yin, B.Q. Xu, C.F. Ng, C.T. Au, Appl. Catal. B: Environ. 48 (2004) 237–241.
[30] S.F. Yin, B.Q. Xu, S.J. Wang, C.F. Ng, C.T. Au, Catal. Lett. 96 (2004) 113–116.
[31] S.F. Yin, B.Q. Xu, W.X. Zhu, C.F. Ng, X.P. Zhou, C.T. Au, Catal. Today 93 (2004) 27–38.
[32] S.J. Wang, S.F. Yin, L. Li, B.Q. Xu, C.F. Ng, C.T. Au, Appl. Catal. B: Environ. 52 (2004) 287–299.
[33] J.Q. Qi, H.Y. Tian, Y. Wang, G.K.H. Pang, L.T. Li, H.L.W. Chan, J. Phys. Chem. B 109 (2005) 14006–14010.
[34] J. Yang, J.Y. Lee, H.-P. Too, J. Phys. Chem. B 109 (2005) 19208–19212.
[35] M.A. Malik, P. O'Brien, N. Revaprasadu, Chem. Mater. 14 (2002) 2004–2010.
[36] Y.H. Deng, D.W. Qi, C.H. Deng, X.M. Zhang, D.Y. Zhao, J. Am. Chem. Soc. 130 (2008) 28–29.
[37] K.P. Velikov, A. Moroz, A. van Blaaderen, Appl. Phys. Lett. 80 (2002) 49–51.
[38] F. Grasset, N. Labhsetwar, D. Li, D.C. Park, N. Saito, H. Haneda, O. Cador, T. Roisnel, S. Mornet, E. Duguet, J. Portier, J. Etourneau, Langmuir 18 (2002) 8209–8216.
[39] S. Dahl, E. Tornqvist, I. Chorkendorff, J. Catal. 192 (2000) 381–390.
[40] Y.X. Li, L.H. Yao, Y.Y. Song, S.Q. Liu, J. Zhao, W.J. Ji, C.T. Au, Chem. Commun. 46 (2010) 5298.
[41] S.H. Joo, P.J. Young, C.K. Tsung, Y. Yamada, P.D. Yang, G.A. Somorjai, Nat. Mater. 8 (2009) 126–131.
[42] X.L. Pan, X.H. Bao, Chem. Commun. 47 (2008) 6271–6275.